Changes in the local structure of a $La_{0.70}Ca_{0.30}MnO_3$ CMR sample induced by a magnetic field

D. Cao,[1] F. Bridges,[1] C. H. Booth,[2] and J. J. Neumeier[3]
[1]*Department of Physics, University of California, Santa Cruz, California 95064*
[2]*Los Alamos National Laboratory, Los Alamos, New Mexico 87545*
[3]*Department of Physics, Florida Atlantic University, Boca Raton, Florida 33431-0991*
(Received 1 November 1999; revised manuscript received 5 June 2000)

We investigated the effect of an applied magnetic field on the local distortions of MnO_6 octahedra in a $La_{0.70}Ca_{0.30}MnO_3$ colossal magnetoresistive (CMR) sample. Previously we have shown that the variance $\sigma^2(T)$ for the Mn-O pair distribution function is a function of the magnetization $M(T)$; however, in the earlier study, each point is at a different temperature. Since an external magnetic field directly controls the sample magnetization, we expect to observe a corresponding change in σ^2 of a CMR sample when a magnetic field **B** is applied at a fixed temperature. Two field-orientations were used with **B** parallel and perpendicular (horizontally) to the x-ray polarization vector **P**. Our measurements verify that the local distortion does indeed change with **B** near T_c, as expected.

I. INTRODUCTION

The substituted manganites $La_{1-x}Ca_xMnO_3$, form colossal magnetoresistive materials for x roughly in the range from 0.2 to 0.5.[1–4] These materials are ferromagnetic metals (FM) at low temperatures below the Curie temperature T_c, and have a metal-to-insulator (MI) transition at a temperature T_{MI}, which is often close to T_c.[5] The large size of the magnetoresistance, particularly in thin-film samples,[6–8] led people to propose that a polaronlike lattice distortion must also be present,[9–13] in addition to the double exchange (DE) interaction.[14–16] Over the last few years such distortions have been observed, and the character and magnitude of these distortions as a function of temperature have now been well-documented by x-ray absorption fine structure (XAFS) experiments and by pair distribution analysis of neutron diffraction data in some colossal magnetoresistive (CMR) systems.[17–23] Such measurements, obtained at zero magnetic field, show that the amplitude of the Mn-O pair distribution peak decreases rapidly with T, for temperatures just below T_c. This change can be modeled as a rapid increase in σ, the width of the pair distribution function, over this temperature range. At higher temperatures the change of σ with temperature is much slower; this leads to a well-defined breakpoint at T_c in a plot[18] of σ^2 vs T.

In our recent XAFS experiments[17,18] we have shown that there is a direct relationship between the magnetization of the sample and changes in the local distortions below T_c. Specifically, $\ln(\Delta\sigma^2)$ is a linear function of the magnetization, where $\Delta\sigma^2$ is defined by the equation

$$\Delta\sigma^2 = \sigma_T^2 + \sigma_{\mathrm{FP}}^2 - \sigma_{\mathrm{data}}^2. \quad (1)$$

Here σ_T^2 is a measure of the phonon contribution (the Debye-Waller contribution), σ_{FP}^2 is the full polaronlike distortion obtained at high temperature, which is defined as the difference between σ_{data}^2 and σ_T^2 at high temperatures (above T_c), and σ_{data}^2 is extracted from fits of the XAFS data,[18,20] for the Mn-O peak. $\Delta\sigma^2$ is zero above T_c and $\ln(\Delta\sigma^2)$ increases linearly as the sample's magnetization increases.[17,18] It is also known that the resistivity is very sensitive to small changes in volume.[24] Thus these relatively larger changes in the local distortion are expected to change the resistivity, and likely modify both the carrier effective mass and mobility.

The logarithmic relationship between local structure and magnetization was obtained from a combination of measurements of σ (measured by XAFS) and of magnetization, each as a function of temperature. However, every data point in such an analysis represents a different temperature. To verify that the local structure is directly related to magnetization, measurements as a function of magnetic field for a fixed temperature are needed. Moreover, such measurements are also necessary for direct comparison to resistivity vs magnetization measurements.[25] In this paper we report our first results of such investigations.

The ferromagnetic transition in these materials is often not sharp. The magnetization is nearly constant at low temperatures and decreases to zero as T approaches T_c, typically over a range of 20–60 K. Magnetization measurements, taken as a function of applied magnetic field, show that the value of T_c increases with external magnetic field.[25] A lowest order approximation is that the magnetization curve is rigidly shifted to higher temperatures. If the local structure is directly connected to magnetization, we expect the breakpoint, in plots of σ^2 vs T, to also shift to higher temperatures; consequently for a given temperature near T_c, σ^2 should decrease when a magnetic field is applied. Here we report our observation of this effect.

Experimental details about the XAFS experiments are given in Sec. II. The XAFS data and the analysis are presented in Sec. III, and the conclusions in Sec. IV.

II. EXPERIMENTAL DETAILS

For the initial experiments reported here, measurements were taken with magnetic fields of either 0 or 1 T, with the magnetic field orientation either parallel or perpendicular (horizontally) to the x-ray polarization vector **P** (see Fig. 1 for orientation details). XAFS is sensitive to distortions primarily along the polarization vector; consequently with two

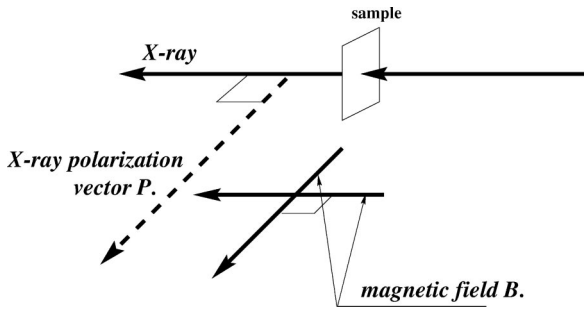

FIG. 1. This plot shows the orientation of the x-ray polarization vector **P** and the two possible orientations of magnetic field **B**.

field orientations we can probe *distortions* that are perpendicular and parallel to the applied field.

The XAFS data were collected at the Stanford Synchrotron Radiation Laboratory (SSRL), using beam line 4-2 (silicon $\langle 220 \rangle$ monochromator crystals) and beam line 10-2 (silicon $\langle 111 \rangle$ monochromator crystals) for the 30% Ca doped LCMO sample. Most of the data points were taken in the vicinity of the transition temperature T_c, with some data collected well above and well below T_c. The sample used for these measurements is the same sample as used previously, with a transition temperatures of 260(2) K; additional sample details are provided in Ref. 18.

The basic principle of XAFS is that when a photoelectron is ejected from an atom by the incoming x ray, the outgoing electron wave will be back scattered by the neighboring atoms. Interference between the outgoing and back-scattered waves modulates the absorption coefficient μ as a function of x-ray energy—i.e., $\mu = \mu_0(1+\chi)$, where μ_0 is a smooth background function[26] and χ is the oscillatory XAFS function. The energy scale is usually converted to k space [$k = \sqrt{2m_e(E-E_0)}/\hbar$, where E_0 is the edge energy] and a theoretical expression for $k\chi$ is given by[27]

$$k\chi(k) = \mathrm{Im} \sum_i A_i \int_0^\infty F_i(k,r) \times \frac{g_i(r_{0i},r) e^{i[2kr + 2\delta_c(k) + \delta_i(k)]}}{r^2} dr, \qquad (2)$$

where the amplitude factor A_i is given by

$$A_i = N_i S_0^2. \qquad (3)$$

N_i is the number of atoms in shell i and S_0^2 is an amplitude reduction factor, which corrects for many-body effects. $F_i(k,r)$ is the back scattering amplitude of the photoelectron wave from shell i with a mean-free path reduction, and $g_i(r_{0i},r)$ is the pair distribution function (assumed here to be Gaussian) for the atoms at r_{0i}. $\delta_c(k)$ and $\delta_i(k)$ are the phase shifts of the photoelectron for the central and backscattering atoms respectively. The program FEFF6 (Ref. 28) provides excellent values for $F_i(k,r)$ and the phase shifts.

III. XAFS DATA

The k-space data for a temperature very close to T_c, are presented in the top panel of Fig. 2 (30% Ca sample); they were collected using silicon $\langle 220 \rangle$ monochromator crystals.

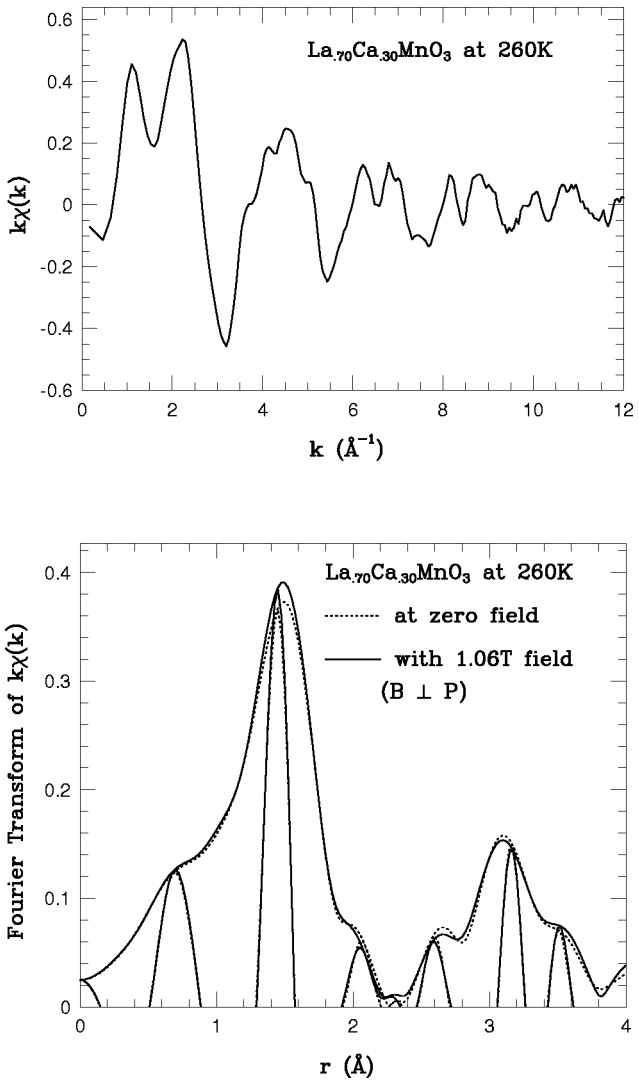

FIG. 2. Top panel is a plot of the k-space data for the 30% sample at $T = 260$ K. Bottom panel shows the Fourier transform of $k\chi$ for the same sample with and without a magnetic field applied (perpendicular to the x-ray polarization vector). There is clearly an increase in amplitude of the first peak (Mn-O) when a magnetic field is applied near T_c.

The y axis represents $k\chi(k)$, with $\chi(k)$ obtained from $\chi(k) = \mu(k)/\mu_0(k) - 1$. In the bottom panel of Fig. 2 we plot the Fourier transform of the k-space data for the same temperature, with and without a magnetic field **B** applied perpendicular to the polarization vector **P** (**B** is parallel to the x-ray beam). This figure shows that there is a small change in the amplitude of the Mn-O (first) peak in the Fourier transform (r-space) data, induced by the application of a magnetic field.

IV. XAFS DATA ANALYSIS

The Mn-O peak was fit in r space using theoretical functions generated by the program FEFF6 (Ref. 28) with the quantity $S_0^2 N$ fixed at 4.3, based on earlier work.[17,18,20] In these fits, only σ and r were varied. The value of σ^2 for the Mn-O peak was obtained for each temperature and magnetic field. Three scans were taken for each configuration and analyzed independently. The root mean square (r.m.s.) variation

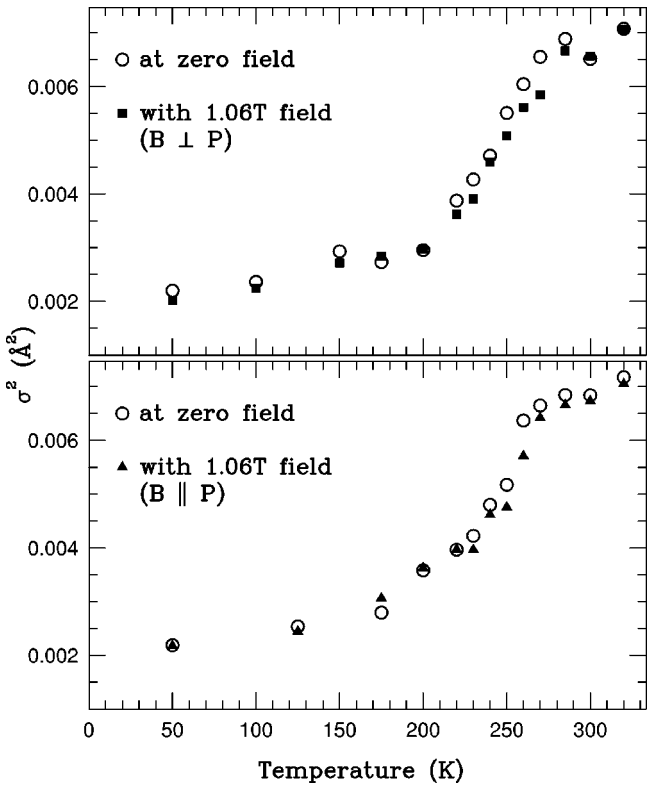

FIG. 3. A plot of σ^2 vs T for the 30% sample, with and without a magnetic field applied both parallel and perpendicular to the x-ray polarization vector. The upper panel shows the case with $B \perp P$ and the bottom panel shows the case with $B \| P$. The error bars of these data points are about the size of the symbols, and are not shown in this figure.

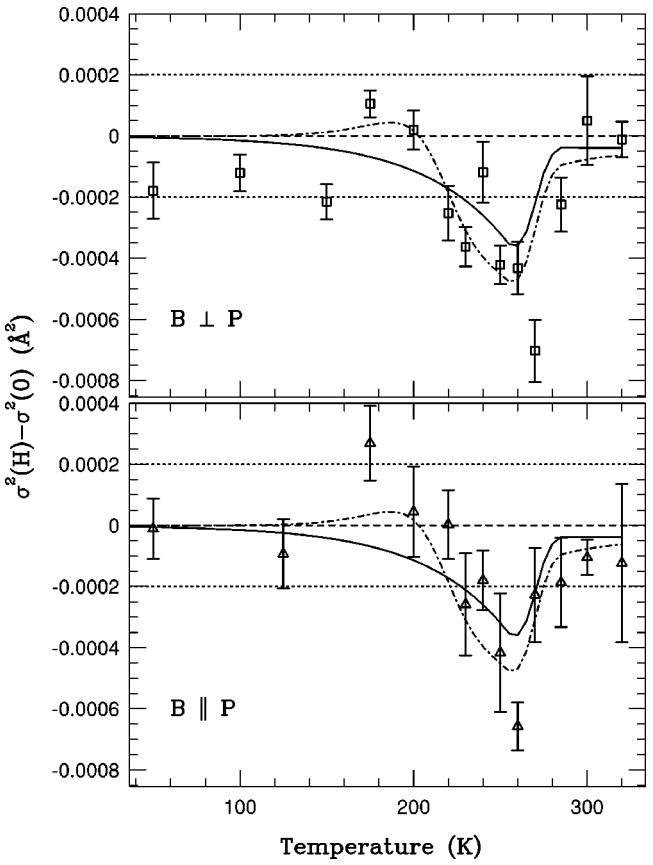

FIG. 4. The difference in σ^2 between $B=1.06$ T and $B=0$ for two field orientations. In both panels, the solid line represents the curve calculated from Eq. (4), with $\Delta T=5$ K for both orientations. The dot-dashed line is a fit to Eq. (5). This fit includes the possibility that the local distortion transition, plotted in Fig. 3, broadens with magnetic field. Again, we plot the same calculated curve for both orientations. The dotted line shows the two-sigma error estimate and the dashed line is the zero line.

of the values of σ^2 from these fits provides an estimate of the relative errors (There is an absolute overall uncertainty in σ^2 of order 10–15%).

In Fig. 3 we plot σ^2 as a function of temperature for the 30% sample (silicon $\langle 220 \rangle$ monochromator crystals), with and without a magnetic field applied perpendicular or parallel to **P**. At low temperatures, there is essentially no change when the magnetic field is applied. A similar result is also obtained well above T_c. However, in a range of temperatures near T_c, the value of σ^2 is clearly decreased when the magnetic field is present. To make this change clearer, we plot in Fig. 4 the difference in σ^2, with and without a magnetic field present for both orientations $[\sigma^2_{\rm diff}=\sigma^2(H)-\sigma^2(0)]$. There is a clear dip in the difference curve that is greater than the two-sigma error estimate, which is indicated by the dotted lines. The results for the field parallel to **P** (perpendicular to the x-ray beam), are also plotted on Figs. 3 and 4; again there is a dip in the vicinity of T_c; the data suggest a slightly smaller dip than the result for the perpendicular (parallel to the x-ray beam) case, but a better signal-to-noise is needed for a definitive conclusion.

Similar measurements were also made for this sample using silicon $\langle 111 \rangle$ monochromator crystals as shown in Fig. 5. In the top panel, the data are plotted as a function of temperature for magnetic fields of 0 and 1 T, and the same two field orientations. Although we have fewer data points for this run, the apparatus/beam was more stable. For this data set, we observed the same general behavior, a dip very close to T_c, and the suggestion of a slight difference in $\sigma^2_{\rm diff}$ for the two field orientations, with $|\sigma^2_{\rm diff}|$ slightly larger when the **B** field is perpendicular to **P**. However, the magnitude of the effect is also a little smaller. In the bottom panel we plot the difference function $\sigma^2_{\rm diff}$, as a function of temperature for the two field orientations, which shows this difference near T_c more distinctly. Again both at low temperatures and at temperatures well above T_c, there is no difference within the relative errors. $|\sigma^2_{\rm diff}|$ has a maximum near 260 K as observed using silicon $\langle 220 \rangle$ monochromator crystals.

One way to begin to model the dip in these plots, is to first consider a rigid shift of the σ^2 vs T plot to higher temperature when a magnetic field is applied, consistent with the shift of T_c observed previously.[25] Then the difference function is approximately given by

$$\delta\sigma^2 = -\frac{\partial(\sigma^2)}{\partial(T)}\Delta T(B). \tag{4}$$

To obtain the derivative function, a smooth curve is first fit to the experimental data. The slope of this curve is then used in Eq. (4) which is plotted in Fig. 4 as a solid line, with $\Delta T \sim 5$ K for both orientations. This functional form fits the difference data moderately well within the relatively large errors, except in a region from roughly 180–210 K. Al-

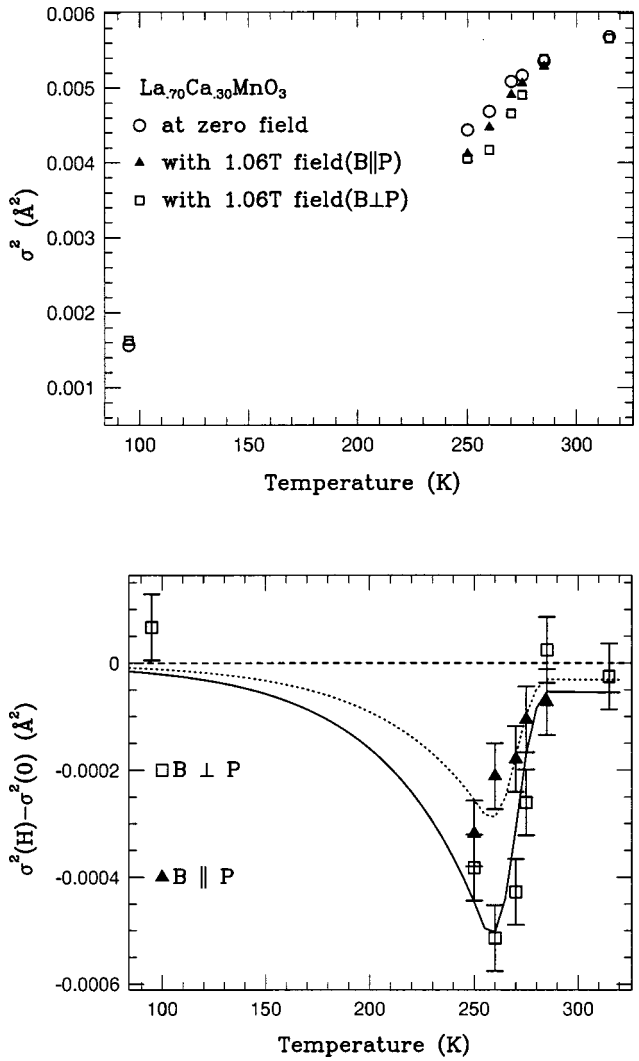

FIG. 5. The upper panel is a plot of σ^2 vs temperature. Data for both orientations of magnetic field (parallel and perpendicular to the x-ray polarization vector) as well as data without a magnetic field are shown in this window. The error bars of these data points are not shown in this window since they are about the size of the symbols. The bottom panel shows the difference in σ^2 between $B=1$ T and $B=0$ as a function of temperature for two field orientations. The solid line and dotted line in this bottom panel show $[\partial(\sigma^2)/\partial(T)]\Delta T(B)$ for $B\perp P$ and $B\|P$, respectively, with $\Delta T=7\pm1$ K and 4 ± 1 K for these two orientations.

though a slightly better fit can be achieved using different values of ΔT for the two orientations, the shift in T_c should be independent of field orientation. This, plus the poor fit in the range 180–200 K indicate that a one-parameter model is too simple to describe the data well. The fact that the data near 190 K lie well above the solid curve suggests that there is also a change in the width (in temperature) of the structural transition, that might in principle be different for the two field orientations. Consequently we consider a model that has both a shift of T_c (same for both field orientations) and a broadening of the transition region. This can be phenomenologically described by adding a function to Eq. (4) that looks, similar to the derivative of a Lorentzian (or Gaussian) function, i.e., a function that is positive below and negative above the transition. Then

$$\delta\sigma^2=-\frac{\partial(\sigma^2)}{\partial(T)}\Delta T_c(B)-A\frac{(T-T_c+B)/W^2}{\{1+[(T-T_c+B)/W]^2\}^2}, \quad (5)$$

where A is an amplitude, W is the effective width, and B determines where the center is relative to T_c. This model is plotted as a dot-dash line in Fig. 4, and fits the data better over the entire T range with the same value of $\Delta T_c(B)$ (5 K) for both field orientations. Here we have also kept A, B, and W the same (0.0183 Å^2, 41.29 K, 42.76 K) for the two field orientations.

In Fig. 5 we only plot the rigid shift model since there is no data below 250 K with which to compare. Here we use two values of ΔT, 4 and 7 K to show the difference in the fit for the two orientations. This data is more suggestive of an orientation dependence but still not conclusive. If this difference is real—i.e., $|\sigma^2_{\rm diff}|$ is larger with the field perpendicular to the x-ray polarization (see bottom panel of Fig. 5)—then this means that there is also a small magnetostrictive effect for these materials, which could be modeled by different values of the parameter W in the above phenomenological model. To have a larger decrease of local distortion when the magnetic field is perpendicular to the polarization vector, would require that distortions perpendicular to the magnetic field are more easily removed, or conversely, that the remaining distortions are preferentially parallel to the applied magnetic field. Another way to view this situation is that within the transition regime (200–260 K), the hopping probability may be slightly different for hopping parallel or perpendicular to the applied **B** field. The sign of the apparent magnetostriction would be consistent with that obtained by Lofland *et al.* in microwave spectroscopy experiments.[29] However, additional experiments using larger magnetic fields will be needed to verify this very tentative result.

In these experiments, it was not possible to investigate how σ^2 varies as a function of the applied magnetic field, because the available magnetic field range was too small. To extend the measurements in this way will likely require fields of 10 T and above. Such measurements would be important for understanding the connections between the local structure, charge, and magnetization. Specifically we need to determine if the changes in the local distortions, induced by a magnetic field, depend primarily on the magnetization or also depend on other parameters such as the conductivity.

V. CONCLUSION

In conclusion, these experiments show directly that the local distortions of the MnO_6 octahedra do change when a magnetic field is applied. The largest changes occur very close to T_c where the temperature dependence of σ^2 is strongest; when the magnetization is zero or when it is near saturation, such as occurs at low temperatures, there is no significant change in the local distortions in the presence of a **B** field.

ACKNOWLEDGMENTS

This work was supported by NSF Grant No. DMR9705117. The experiments were performed at SSRL, which is operated by the U.S. DOE, Division of Chemical Sciences, and by the NIH, Biomedical Resource Technology Program, Division of Research Resources.

[1] E.O. Wollan and W.C. Koehler, Phys. Rev. **100**, 545 (1955).
[2] G.H. Jonker and J.H. van Santen, Physica (Amsterdam) **16**, 337 (1950).
[3] G.H. Jonker, Physica (Amsterdam) **22**, 707 (1956).
[4] P. Schiffer, A.P. Ramirez, W. Bao, and S-W. Cheong, Phys. Rev. Lett. **75**, 3336 (1995).
[5] A.P. Ramirez, J. Phys.: Condens. Matter **6**, 8171 (1997).
[6] R.M. Kusters, J. Singleton, D.A. Keen, R. McGreevy, and W. Hayes, Physica B **155**, 362 (1989).
[7] R. von Helmolt, J. Wecker, B. Holzapfel, L. Schultz, and K. Samwer, Phys. Rev. Lett. **71**, 2331 (1993).
[8] S. Jin, M. McCormack, T.H. Tiefel, R.M. Fleming, J. Phillips, and R. Ramesh, Science **264**, 413 (1994).
[9] A.J. Millis, P.B. Littlewood, and B.I. Shraiman, Phys. Rev. Lett. **74**, 5144 (1995).
[10] H. Röder, J. Zang, and A.R. Bishop, Phys. Rev. Lett. **76**, 1356 (1996).
[11] A.J. Millis, B.I. Shraiman, and R. Mueller, Phys. Rev. Lett. **77**, 175 (1996).
[12] A.J. Millis, Phys. Rev. B **53**, 8434 (1996).
[13] A.J. Millis, R. Mueller, and B.I. Shraiman, Phys. Rev. B **54**, 5405 (1996).
[14] C. Zener, Phys. Rev. **82**, 403 (1951).
[15] P.W. Anderson and H. Hasegawa, Phys. Rev. **100**, 675 (1955).
[16] P.G. de Gennes, Phys. Rev. **118**, 141 (1960).
[17] C.H. Booth, F. Bridges, G.H. Kwei, J.M. Lawrence, A.L. Cornelius, and J.J. Neumeier, Phys. Rev. Lett. **80**, 853 (1998).
[18] C.H. Booth, F. Bridges, G.H. Kwei, J.M. Lawrence, A.L. Cornelius, and J.J. Neumeier, Phys. Rev. B **57**, 10 440 (1998).
[19] S.J.L. Billinge, R.G. DiFrancesco, G.H. Kwei, J.J. Neumeier, and J.D. Thompson, Phys. Rev. Lett. **77**, 715 (1996).
[20] D. Cao, F. Bridges, D.C. Worledge, C.H. Booth, and T. Geballe, Phys. Rev. B **61**, 11 373 (2000).
[21] D. Cao, F. Bridges, A. P. Ramirez, M. Olapinski, M. A. Subramanian, C. H. Booth, and G. Kwei (unpublished).
[22] G. Subías, J. García, M.G. Proietti, and J. Blasco, Phys. Rev. B **56**, 8183 (1997).
[23] T.A. Tyson, J. Mustre de Leon, S.D. Conradson, A.R. Bishop, J.J. Neumeier, H. Röder, and J. Zang, Phys. Rev. B **53**, 13 985 (1996).
[24] J.J. Neumeier, K. Andres, and K.J. McClellan, Phys. Rev. B **59**, 1701 (1999).
[25] M.F. Hundley, M. Hawley, R.H. Heffner, Q.X. Jia, J.J. Neumeier, J. Tesmer, J.D. Thompson, and X.D. Wu, Appl. Phys. Lett. **67**, 860 (1995).
[26] J.J. Rehr, C.H. Booth, F. Bridges, and S.I. Zabinsky, Phys. Rev. B **49**, 12 347 (1994).
[27] C.H. Booth, F. Bridges, J.B. Boyce, T. Claeson, B.M. Lairson, R. Liang, and D.A. Bonn, Phys. Rev. B **54**, 9542 (1996).
[28] S.I. Zabinsky, J.J. Rehr, A. Ankudinov, R.C. Albers, and M.J. Eller, Phys. Rev. B **52**, 2995 (1995).
[29] S.E. Lofland, S.M. Bhagat, H.L. Ju, G.C. Xiong, T. Venkatesan, R.L. Greene, and S. Tyagi, J. Appl. Phys. **79**, 5166 (1996).